AIAA Propulsion and Energy Forum
19-22 August 2019, Indianapolis, IN
AIAA Propulsion and Energy 2019 Forum

10.2514/6.2019-4080

Stationary Profiles and Axial Mode Oscillations in Hall Thrusters

Andrei Smolyakov*, Ivan Romadanov† and Oleksandr Chapurin‡
University of Saskatchewan, 116 Science Place, Saskatoon SK, S7N 5E2 Canada

Yevgeny Raitses§
Plasma Physics Laboratory, Princeton University, Princeton, New Jersey 08543, USA

Gerjan Hagelaar¶ and Jean-Pierre Boeuf‖
CNRS, LAPLACE, Bât 3R2, Université Paul Sabatier, 31062 Toulouse Cedex 9, France

The axial modes (and breathing mode in particular) are among the most violent oscillation modes in Hall thruster. Breathing mode is manifested by strong fluctuations of discharge current and other plasma parameters. It is generally understood as the instability associated with ionization and neutral depletion processes in the thruster channel, but a number of other effects, such as temperature evolution and boundary conditions are also important. Despite long history of studies, exact physical mechanisms and conditions for the instability are not well understood. Within one-dimensional model we have proceeded to study the general case of axial mode instabilities starting from of stationary (time-independent) solutions. The nature and typical characteristics of stationary solutions are established with analytical analysis. It is shown that the existence of the singular sonic point results in "stiff" profiles of the accelerating electric field and other plasma parameters. Such "stiff" profiles have global nature, in particular, show strong dependence on boundary conditions on the anode. Using fluid and hybrid (fluid electrons and kinetic ions/neutrals) simulations we have studied the axial stability of such global profiles. It is shown that axial instabilities are sensitive to the electron/mobility and magnetic field as well as the electron temperature evolution model and losses.

I. Nomenclature

A	=	cross section area of a Hall thruster
α	=	coefficient to electron wall collision frequency
β	=	ionization rate coefficient
β_a	=	coefficient to anomalous Bohm frequency
b_v	=	Bohm velocity factor
B	=	axial distribution of radial magnetic field
c_s	=	ion-sound velocity
e	=	elementary charge
E	=	axial electric field
ε	=	electron energy
J_a	=	atom density flux
J_d	=	total (electron and ion) discharge current flux
J_T	=	total (electron and ion) discharge current density
I_D	=	total (electron and ion) discharge current

*Professor, Department of Physics and Engineering Physics
†PostDoctoral Fellow, Nova Scotia Health Authority, 1276 South Park St, Halifax NS, B3H 2Y9 Canada
‡PhD student, Department of Physics and Engineering Physics
§Senior Scientist, Princeton Plasma Physics Laboratory
¶Directeur de Recherche, CNRS, LAPLACE
‖Directeur de Recherche CNRS, LAPLACE

k_m	=	electron neutral collision rate constant
K	=	electron collisional energy loss coefficient
L	=	channel length
μ_e	=	electron mobility
m_e	=	electron mass
m_i	=	Xenon ion mass
$\dot{m}$	=	atom mass flow rate
n	=	plasma density (quasineutral)
n_e	=	electron density
n_i	=	ion density
n_i'	=	ion density axial derivative at the sonic point
n_s	=	plasma density (quasineutral) at the sonic point
N	=	atom density
ν_m	=	total electron momentum exchange frequency
ν_{en}	=	electron-neutral collision frequency
ν_{walls}	=	electron-wall collision frequency
ν_B	=	anomalous Bohm electron frequency
ν_ε	=	coefficient to anomalous electron energy losses
p_e	=	electron isotropic pressure
q_e	=	electron heat flux
T_e	=	electron temperature
U	=	a constant in electron anomalous energy losses coefficient
ϕ	=	electric potential
ϕ'	=	electric potential axial derivative at the sonic point
v_a	=	atom average velocity
v_i	=	ion average velocity
v_{ex}	=	electron average velocity in axial direction
v_i'	=	ion velocity axial derivative at the sonic point
W	=	electron anomalous energy loss coefficient
ω_{ce}	=	electron-cyclotron frequency
x	=	axial coordinate

II. Introduction

Ubiquitous axial breathing mode is one of the powerful nonlinear instabilities observed in Hall thrusters. Though most easily seen in oscillations of the discharge current, it also involves fluctuations of other thruster parameters such as ion, and neutral density, electric field, ion velocity and electron temperature. Despite long history of experimental and theoretical studies the exact role of various plasma parameters on breathing mode remains unclear. Neither, the exact conditions for breathing mode excitation are understood at this time.

Since the frequency of a typical breathing mode (10-20 kHz) is within the range of ionization frequencies, one expects that depletion of neutral density due to ionization is one of the important ingredients of the breathing mode. Coupling of neutral and ion (plasma) densities lead to a simple zero-dimensional predator-prey model [1] in which the full length of the ionization zone is replaced by the boundary values of the neutral and ion densities at the anode and the end of the ionization zone assuming the constant values of the ion and neutral velocities [1, 2]. Various modification of the predator-prey model were suggested later. One of the major problem of the zero-dimensional predator-prey model is that stable oscillations predicted by such model are not reproduced in the system of one-dimensional differential equations for neutral and ion densities with the same boundary conditions. Moreover, using the value of the neutral density at the anode as an oscillating variable (as in the original model [1]) is inconsistent with the constant flux (and the velocity) of the injected neutrals. It was suggested to use the fixed neutral density at the anode, while the neutral density at the exit end of the zone became a time dependent variable [3]. It was shown that oscillations are damped in such model, but the inclusion of the electron energy makes oscillations unstable [3]. The authors of Refs. [4–6] proposed to use the electron (instead of ion) continuity equation, and the electron velocity in the drift-diffusion approximation, with the motivation that that electron mobility strongly affects the breathing mode.

It has been recognized [7] that self-consistent dynamics of the electric field is important for axial ionization modes. In such model [7–9] the ion and neutral dynamics is complemented with the electron equation (Ohm's law) and the evolution of the electric field is determined by the quasineutrality constraint so that the total current is uniform. In hybrid models, the ion dynamics is described kinetically [9–11] while the fluid model is used for electrons. The evolution of the electron temperature was included in Refs. [9–11] in the lowest order (neglecting the electron heat flux), and the electron diffusion in the Ohm's law was also neglected. Complex pattern of unstable oscillations was observed and by adjusting the value of the electron mobility, one can get the resulting oscillations close to the observed experimental data [9, 10]. The authors of Ref. [11] have studied the linear instabilities in this model and have concluded that the resistive instability is a critical element that triggers the fluctuations of the electric field: increase of the electric field results in larger electron temperature, leading to enhanced ionization and depletion of the neutral density.

The resistive axial instability [11–13]occurs due to differential drift of the electron and ions and different nature of the electron and ion response. The electron response is dissipative (the electron velocity is due to mobility) and the velocity is in phase with the electric field. The ions are in the ballistic regime, so that the ion velocity is in phase with the perturbations of the potential. The phase shift between ion and electron fluctuations results in positive feedback leading to the instability [13]. The competition of the electron and ion equilibrium flow may result in the lower real part of the frequency and even to the change in the direction of the mode propagation (from the ion to the electron velocity direction). Instabilities within similar fluid model were considered in Ref. [14], but thought to be of higher frequencies in the ion transit-time range. It was noted in Ref. [15] that the electron energy evolution brings additional unstable modes of the transit-time nature.

General fluid equations including ionization were analyzed in Ref. [16] using the time scale separation valid for low frequency ionization mode. It was proposed that that the evolution of the ionization (breathing) mode can be split from other instabilities effectively reducing it to the predator-prey type cycle [16, 17].

At this time, there is large number of models proposed to characterize the breathing mode oscillations [18]. These models vary from relatively simple zero-dimensional predator-prey type equations [19–21] to complex systems of fluid equations that may include the (electron) energy evolution with heat flux, particle and energy wall and anomalous losses [22, 23], ion energy evolution [24], neutral-wall collisions, multi-step ionization and induced magnetic field effect [25]. A sub-class of the models use the kinetic approach to describe the ions and neutrals behavior [10, 22, 23, 25, 26]. In general, these models exhibit high sensitivity to various input variables, such as electron mobility (which has to be taken anomalous in most cases), particle and energy losses and other plasma parameters.

Our analysis indicates that stationary solutions in this problem have complex structure and also sensitive to variations of plasma parameters. The complex structure of stationary solutions is related to the well known problem in the acceleration of ions by the electric field in quasineutral plasma, namely the transition via the sonic point: the point where the local ion velocity is equal to the local ion-sound velocity. The importance of this transition has been noted in studies of stationary plasma profiles [27–30]. The condition that no singularity occurs at the point $v_i = c_s$ imposes certain constraints on plasma parameter making the whole problem of stationary plasma profiles global, which is reflected in the numerical stiffness of the solution. One consequence of this is that the boundary conditions affect plasma profile globally across the full length of the thruster. A related problem may occur near the anode sheath where the singular point $v_i = -c_s$ is possible. Motivated by these observations, in this paper we investigate the role of boundary conditions on the axial modes that involve ionization.

To clarify the role of the sonic points, we first study the structure and type of global stationary profiles. These profiles are then used to study the excitation of breathing mode fluctuations. It is important to note that here we deal with convective versus absolute instabilities and Fourier mode analysis for breathing mode does not provide full information[31]. We employ the initial value numerical simulations to study the stability of stationary solutions (found by different methods from stationary equations). It is found that some stationary solutions represent a global minima so they can be reached from arbitrary initial state. We investigate the role of boundary conditions on the breathing mode oscillations and show that boundary conditions for the quasineutral region affect the instabilities.

III. The steady-state solutions and sonic point transition

Here, we analyze stationary plasma flow at given values of the discharge current I_D and the neutral flux J_a. Our emphasis is on the constraints imposed by the regularity condition at $v_i = c_s$. Stationary profiles were considered earlier and the role of a singular point was considered [27, 28, 32], however explicit constraints imposed by the regularity conditions were not discussed. For simplicity, here we consider the isothermal case, so temperature is assumed constant and uniform in space. We also neglect plasma losses. Stationary equations are written as follows

$$v_a \frac{\partial N}{\partial x} = -\beta N n, \tag{1a}$$

$$\frac{\partial}{\partial x}(n_i v_i) = \beta N n_i, \tag{1b}$$

$$v_i \frac{\partial v_i}{\partial x} = -\frac{e}{m_i}\frac{d\phi}{dx} + \beta N(v_a - v_i), \tag{1c}$$

$$\frac{d\phi}{dx} = -\frac{J_d}{n_i \mu_e} + \frac{v_i}{\mu_e} + \frac{1}{e n_i}\frac{\partial T_e n_i}{\partial x}, \tag{1d}$$

where the total discharge current flux is $J_d = n_i v_i - n_e v_e$, and the neutral density N can be deduced from the equation $N = \dfrac{\dot{m}}{m_i v_a A} - \dfrac{n_i v_i}{v_a}$. The mass flux is defined from the latter equation as $J_a = n v_a = \dfrac{\dot{m}}{m_i A}$. Here, β is the ionization rate, μ_e is the electron mobility perpendicular to the magnetic field, v_a is the neutral flow velocity, T_e is the electron temperature. These equations imply quasi-neutrality $n_i = n_e = n$. The diffusion term $\dfrac{1}{en}\dfrac{\partial T_e n}{\partial x}$ in Ohm's law is important to describe the plasma flow in the anode region and also results in the sonic point singularity.

The electron mobility μ_e is given by the classical expression for collisional transport in the transverse magnetic field:

$$\mu_e = \frac{e}{m_e \nu_m}\frac{1}{1 + \omega_{ce}^2/\nu_m^2}, \tag{2}$$

where $\omega_{ce} = eB/m_e$ is the electron cyclotron frequency and ν_m is the total electron momentum exchange collision frequency. In general, ν_m is

$$\nu_m = \nu_{en} + \nu_{walls} + \nu_B, \tag{3}$$

where ν_B is the anomalous cross-field transport due to field fluctuations and ν_{walls} is the collision frequency with walls. In this however, classical value of the electron mobility was used. From this a set of three ordinary differential equations for the derivatives of v_i, n_i, and ϕ can be derived

$$(c_s^2 - v_i^2)\frac{dv_i}{dx} = \beta n_a c_s^2 - \beta n_a v_i(v_a - v_i) + \nu_e^* \nu_e v_i \equiv F_1(n, J_d, J_a), \tag{4a}$$

$$(c_s^2 - v_i^2)\frac{dn}{dx} = \beta n_a n(v_a - 2v_i) - \nu_e^* n \nu_e \equiv F_2(n, J_d, J_a), \tag{4b}$$

$$(c_s^2 - v_i^2)\frac{e}{m_i}\frac{d\phi}{dx} = \beta n_a c_s^2(v_a - 2v_i) - \nu_e^* \nu_e v_i \equiv F_3(n, J_d, J_a), \tag{4c}$$

where $c_s^2 = T_e/m_i$, $\nu_e^* \simeq \omega_{ce}\omega_{ci}/\nu_e$. The right hand side of these equations depend on two parameters and the density at the critical point, which fully define the operational space: J_d and J_a. The density $n = n_s$ is defined by the condition that the sonic point has no singularity which requires $F_1(n, J_d, J_a) = F_2(n, J_d, J_a) = F_3(n, J_d, J_a) = 0$. These equations lead to the following condition for the density

$$\beta \mu_e c_s (v_a - 2c_s) n_s^2 + (c_s v_a + \beta \mu_e J_a (2c_s - v_a)) n_s - J v_a = 0. \tag{5}$$

This is a quadratic equation, which gives two values of n_s for given values of J_a and J_d. When J_d and J_a are given, one finds n_s from (5). The value of ϕ' can be obtained from the Eq. (4c) after n_i and v_i are known. When the functions $F_1\,(n, J_d, J_a)$, $F_2\,(n, J_d, J_a)$ and $F_3\,(n, J_d, J_a)$ are expanded near the point $v_i = c_s$, the following equation for $v_i' = \partial\phi/\partial x$ is obtained

$$\begin{aligned} &v_i'^2 + v_i'\left[\beta n_a\left(1 - \frac{v_a}{2c_s}\right) + \nu_e^*\left(1 - \frac{J_d}{nc_s}\right)\right] \\ &+\frac{1}{2}\nu_e^*\beta n_a \frac{J_d}{nc_s} + \frac{1}{2}\beta^2 n_a n\left(1 - \frac{2c_s}{v_a}\right) = 0. \end{aligned} \tag{6}$$

This is the quadratic equation as well, so two roots for the derivatives v_i', n_i' and ϕ' are possible for each value of n_s. Once v_i', n_i' and ϕ' are determined, one can integrate the equations (4a-4c) from the point $v_i = c_s$ in both directions. The further constraints are imposed by boundary conditions at the anode side (to the left from the singular point), the global conditions of the discharge length and the applied voltage.

The flow acceleration from the subsonic to supersonic regimes (via the sonic point) in Hall thrusters is somewhat similar to the gas acceleration in the Laval nozzle. The singular point must be maintained regular, which requires that the RHS of Eqs (4) is at the sonic point. This is the condition that makes the solution stiff across the whole length from the anode to the cathode stiff therefore restricting the possible choice of boundary conditions.

For numerical estimates we used plasma parameters typical for the cylindrical Hall thruster. Electron temperature T_e was taken constant along the channel, what implies that the ionization rate coefficient β is constant as well. All parameters are summarized in the Table 6.1 in Ref. [33].

In general, the boundary conditions at the left side can be affected by the anode sheath. We note here that in quasineutral model, there is no natural sheath potential drop due to predominant loss of electrons. The sheath like profile is maintained by the large density gradient inward (density increasing from the left boundary), as a result the electric field near anode may reverse sign to maintain the total current constant. The negative electric field (toward the anode) may result in another singularity $v_i = -c_s$ at the boundary. Sheath and no-sheath solutions have been discussed in the literature and observed experimentally [30, 34–36]. Therefore we allow for general situation with $v_i \geq -c_s$ and consider how does the condition on the anode sheath boundary (specifically, the value of the velocity at the boundary) affect stationary solutions and their stability.

IV. Stationary solutions in operational space diagram and their axial stability

A. Discharge current and injection rate operational space diagram

Important point is that real solutions for n_s, v_i', n_i' and ϕ', exist only in a certain range of the values of J_a and J_d, which can be easily found from the quadratic equation. Here we give examples of n_s, v_i', n_i', and ϕ' diagrams, calculated for parameters from the Ref. [33]. For each value of n_s, the v_i', n', ϕ' derivatives are calculated, and stationary solutions were obtained by the integration from the sonic point in both directions: to the anode and to the cathode. Integration was done from 0 to $-L$ and from 0 to L, where 0 is the location of the sonic point. When integration was done in a negative direction, it was stopped after the ion velocity reached $-c_s$ value, so the solution is obtained over the interval X larger than the thruster length L. By selecting the interval of the given length L, various possible solutions with different values of the potential difference across can be defined. The selection both the length L and the potential difference defines a unique solution.

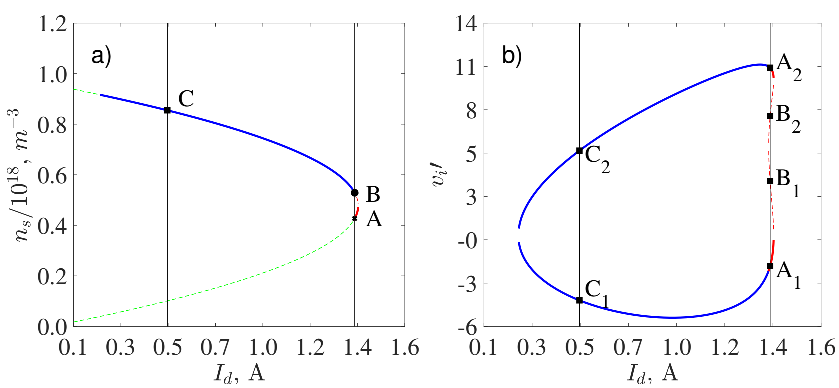

Fig. 1 Diagrams of a) n_s and b) v_i' as functions of the discharge current I_D at fixed value of J_a. Two roots in v_i' correspond to one value of n_s from the high density branch. Only small portion of the lower density branch has real solutions for v_i', such as points A and B.

Different types of the solution are presented in Figs. 1a and 1b as a function of I_d, at a fixed value of J_a. Here $I_D = eJ_dA$, where A is a thruster channel cross-section. For a fixed J, there is a maximum value of J_a for which the solutions exist, 1. For the values of the current smaller than some maximum value, equation 5 has two roots: high density and low density branches. However, for large fraction of the lower density branch the corresponding values of the velocity, density and potential gradients become complex which means absence of the solutions in this region, which is shown by dashed-green line in Fig. 1a and in the Fig. 3), which was zoomed-in and rescaled figure 3.

The high density "n_s" root "C", corresponding to the lower current I_D, generates two different real roots for v_i', n', and ϕ' - "C_1" and "C_2". The profiles of the ion velocity, density and potential for these roots are shown in Fig. 2. One of these solutions, shown as "C_2" is decelerating and is of no interest for the thrusters. The v_i profile for "C_1" root shows supersonic ion acceleration. It is shown here as starting from $-c_s$ condition at the anode sheath boundary, but other choices are possible with different value of the discharge voltage.

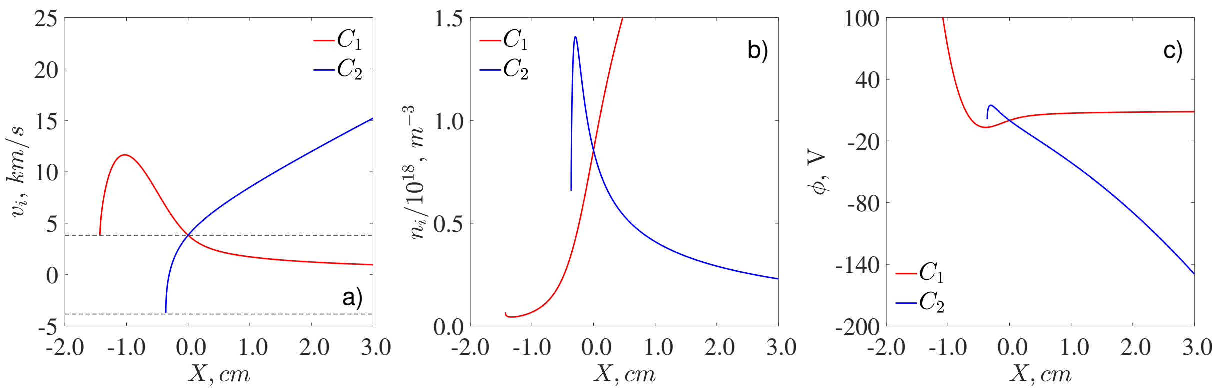

Fig. 2 a) Velocity v_i, b) density n_i, and c) potential ϕ profiles for the root "C". Dashed lines are the ion sound velocity level– $\pm c_s$.

For the higher values of the current, I_d, closer to the maximum value, situation looks more complex. Here, there are two roots for the density and, correspondingly, there are four possible real solutions for the velocity derivative (two for each values of density). These are shown in Fig. 1b and, schematically, in Fig.3, as A_1, A_2, B_1, and B_2. Only one of these is compatible with the accelerating solution and boundary condition at the anode; this solution is very similar to C_2. The other solutions (not shown here) are either decelerating, or cannot be continued below the $v_i = c_s$ velocity and cannot be matched to the condition at the anode.

In summary, it was found that for the given value of the mass flux J_a there exists a range of the discharge fluxes J_d, where a single solution with accelerating ions exists, this region marked solid blue in Fig. 3, not to scale; for some range of the J_a and J_d values, there are no solutions, marked as dashed-green, and in some region, with the current close to the maximum, there are four solutions, marked in solid and dashed red in Fig. 3.

B. Stability and the nonlinear axial modes oscillations

We have studied the stability of obtained stationary profiles in time-dependent simulations. Here we report only the cases with standard Bohm condition at the left boundary, $v_i = -c_s$. Nonlinear initial value time-dependent simulations were performed with the obtained stationary profiles (with corresponding boundary conditions) an an initial state.

Depending on the parameters of stationary solutions, we have identified four distinctly different situations, summarized in diagram Fig.4, not to scale.

For lower values of the discharge current (Zone 1) the stationary profiles remain stable and there are no current oscillations in this region. The discharge current oscillations appear for J_d in Zone 2. It is important to note that the nature of oscillations, as well as their amplitude and frequency, changes as the value of J_d increases. At the beginning of the Zone 2, for lower values of J_d, the oscillations have small amplitude and frequency (see Fig. 5a, b) and have well pronounced single frequency (see Fig. 5a, d). Closer to the end of Zone 2, oscillations amplitude and frequency grow. In Zone 3, there is a transition to multimode oscillations (see Fig. 5b, e) with further increase of amplitude and frequency. At the end of Zone 3 oscillations amplitude reaches its maximum, however, oscillations become strongly non-linear with and the frequency is sharply reduced.

V. Fluid and hybrid modeling of the axial modes dynamics with the electron energy evolution

Here we present a self-consistent one-dimensional axial model that includes additional physical elements such as wall energy losses and electron energy evolution. The simulations were performed with full fluid model and hybrid model,

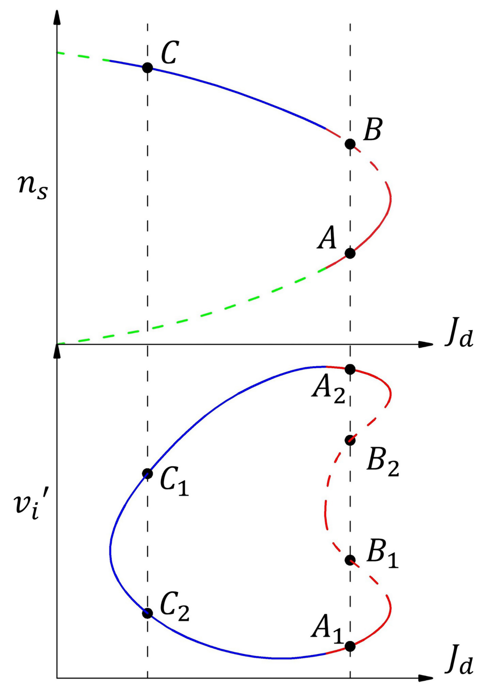

Fig. 3 Diagrams for n_s (top) and v_i' (bottom) as functions of the discharge flux J_d at a fixed value of J_a, not to scale: Dashed-green – no real solutions. Solid blue – two roots, one of which is the expected solution corresponding to the ion acceleration. Red (dashed and solid) – the regions with four solutions, only A_2 root corresponds to the good accelerating solutions.

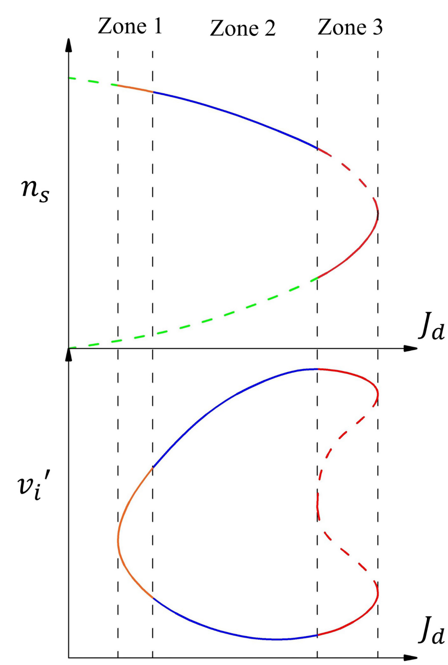

Fig. 4 Stability diagram of stationary solutions in the n_s/v_i', J_d space at a fixed value of J_a. In Zone 1 (orange solid), there are no oscillations. In Zone 2 (blue solid), there exist strongly coherent oscillations. In Zone 3 (red solid and dashed), the multimode oscillations are present.

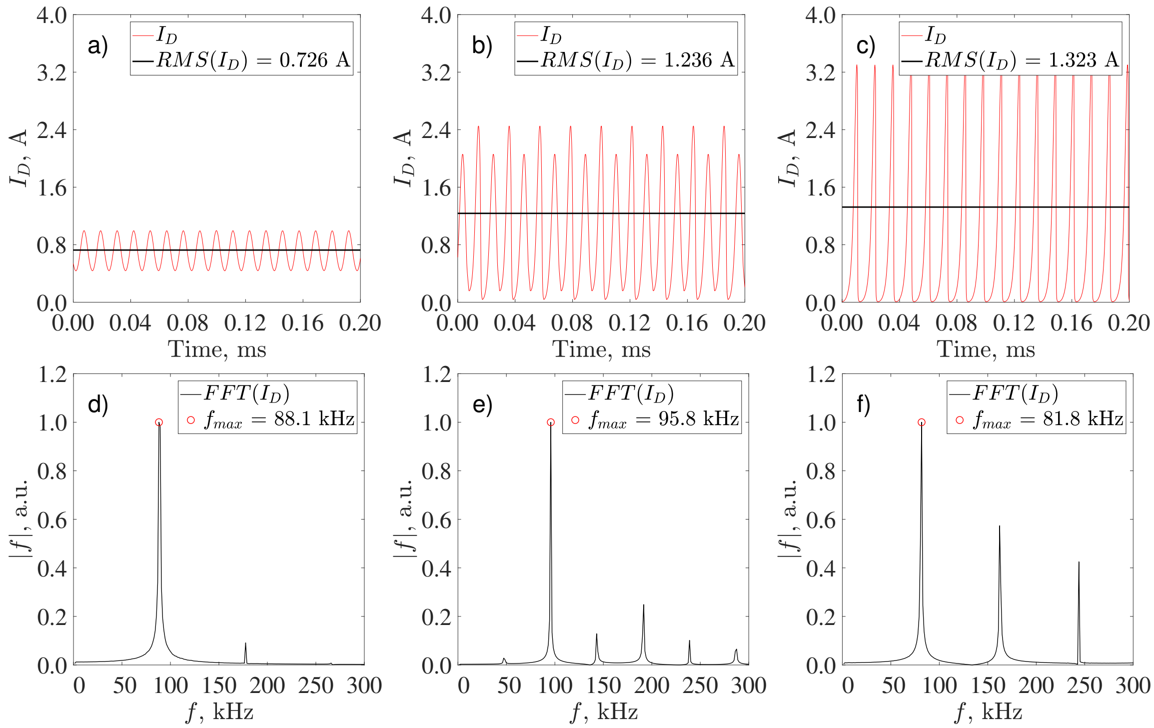

Fig. 5 Discharge current time traces (a-c) and corresponding Fourier spectra (d-f) for different regimes of I_D.

where ions and neutrals are modeled as particles (particle-in-cell method). BOUT++ computational framework[37] was used for full fluid simulations, as in Section IV. Hybrid simulations were performed with the code developed at LAPLACE laboratory, France [10, 22, 23, 38]. One of the goals was to compare the results of fluid and hybrid simulations and study the role of boundary conditions, which for ions can be chosen rather arbitrary in fluid code. Such freedom of boundary conditions is absent in the kinetic ion model. The model and parameters of the simulations are chosen to correspond to the one of LANDMARK benchmarking cases [39].

A. Basic model equations

In the fluid model, neutral dynamics is modeled with the simple advection equation

$$\frac{\partial N}{\partial t} + v_a \frac{\partial N}{\partial x} = -\beta N n, \tag{7}$$

where v_a is a constant. Ion dynamics is described with basic equations for cold unmagnetized ions

$$\frac{\partial n_i}{\partial t} + \frac{\partial}{\partial x}(n_i v_i) = \beta N n_i, \tag{8}$$

$$\frac{\partial v_i}{\partial t} + v_i \frac{\partial v_i}{\partial x} = \frac{e}{m_i} E - \beta N v_i, \tag{9}$$

where we include the ionization source term $\beta n_n n_i$ with ionization coefficient β; omit the pressure term, viscosity tensor in momentum equation; and temperature evolution. Electron dynamics is given by:

$$\frac{\partial n_e}{\partial t} + \frac{\partial}{\partial x}(n_e v_e) = \beta n_n n_e, \tag{10}$$

$$0 = -\frac{e}{m_e} E - \frac{e}{m_e} (\mathbf{v}_{e\perp} \times \mathbf{B})_x - \frac{1}{n_e m_e} \frac{\partial (n_e T_e)}{\partial x} - \nu_m v_{ex}, \tag{11}$$

$$\frac{3}{2}\frac{\partial}{\partial t}(nT_e) + \frac{5}{2}\frac{\partial}{\partial x}(n_e v_{ex} T_e) + \frac{5}{2}\frac{\partial q_e}{\partial x} = -n_e v_{ex} \frac{\partial \phi}{\partial x} - n_e n_a \mathrm{K} - n\mathrm{W}, \tag{12}$$

where ν_m is the total electron momentum exchange frequency, W is the anomalous energy loss coefficient, K is the collisional energy loss coefficient, q_e is the electron heat flux.

$$\mathrm{W} = \nu_\varepsilon \varepsilon \exp(-U/\varepsilon), \tag{13}$$

where $\varepsilon = 3/2T_e$, $U = 20$ eV. Heat flux across magnetic field is

$$q_e = -\mu_e n T_e \frac{\partial T_e}{\partial x}. \tag{14}$$

From Eq. (11) we express the electron velocity as

$$v_{ex} = -\mu_e E - \frac{\mu_e}{n_e}\frac{\partial p_e}{\partial x}, \tag{15}$$

where the electron mobility μ_e given by Eq.3.

and the total electron momentum exchange collision frequency is

$$\nu_m = \nu_{en} + \nu_{walls} + \nu_B, \tag{16}$$

where the electron-neutral collision frequency ν_{en}, electron-wall collision frequency ν_{walls}, and anomalous Bohm frequency ν_B are given with:

$$\nu_{en} = k_m n_a, \tag{17}$$

$$\nu_{walls} = \alpha 10^7 \ [\mathrm{s}^{-1}], \tag{18}$$

$$\nu_B = (\beta_a/16)\, eB/m_e. \tag{19}$$

where $k_m = 2.5 \times 10^{-13}$ $\mathrm{m}^{-3}\mathrm{s}^{-1}$, α and β_a are adjusting constants.

The profile of external magnetic field is shown if Fig. 6, with the channel's exit in the peak of magnetic field intensity. For this electron mobility model we will use different parameters inside and outside the channel, the near wall conductivity contribution $\alpha_{in} = 0.2$, $\alpha_{out} = 0$. The anomalous contribution is set to $\beta_{a,in} = 0.1$, $\beta_{a,out} = 1$.

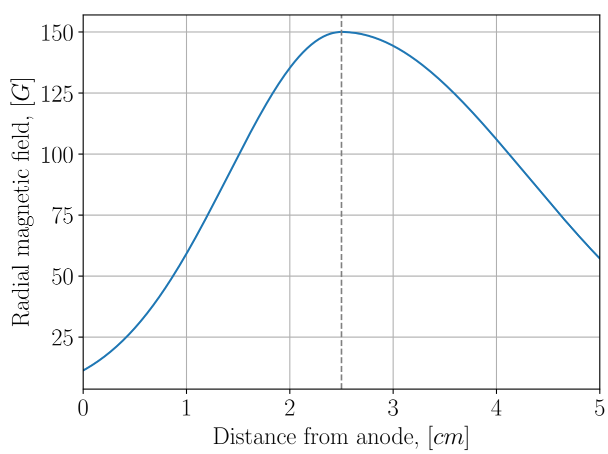

Fig. 6 The magnetic field profile used in simulations, with the channel exit located 2.5 cm **from anode (dashed line).**

We will assume plasma quasineutrality and neglect a potential drop on the Debye sheath near the anode. The total (discharge) current density J_T is determined from the condition

$$\int_0^L E dx = U_0, \tag{20}$$

and given as

$$J_T = \frac{U_0 + \int_0^L \left(\frac{v_i}{\mu_e} + \frac{1}{n} \frac{\partial p_e}{\partial x} \right) dx}{\int_0^L \frac{dx}{en\mu_e}}. \tag{21}$$

Therefore, the full system of equations to be solved,

$$\frac{\partial N}{\partial t} + v_a \frac{\partial N}{\partial x} = -\beta N n, \tag{22}$$

$$\frac{\partial n}{\partial t} + \frac{\partial}{\partial x} (n v_i) = \beta N n, \tag{23}$$

$$\frac{\partial v_i}{\partial t} + v_i \frac{\partial v_i}{\partial x} = \frac{e}{m_i} E - \beta N v_i, \tag{24}$$

$$\frac{3}{2} \frac{\partial}{\partial t} (n T_e) + \frac{5}{2} \frac{\partial}{\partial x} (n v_e T_e) + \frac{5}{2} \frac{\partial q_e}{\partial x} = n v_e E - n n_a \mathrm{K} - n \mathrm{W}, \tag{25}$$

where the electric field E is obtained from the electron momentum Eq. (15). This system is solved with the following boundary conditions. A constant mass flow rate determines the value of n_a at the boundary, as well as recombination of plasma that flows to the anode, hence the boundary condition:

$$N(0) = \frac{\dot{m}}{m_i A v_a} - \frac{n v_i(0)}{v_a}. \tag{26}$$

Bohm type condition for ion velocity can be imposed at the anode $v_i(0) = -b_v \sqrt{T_e/m_i}$, where $b_v = 0$–1 is the Bohm velocity factor which can be varied. Both anode and cathode electron temperature are fixed with $T_e(0) = T_e(L) = 2$ eV. All other boundary conditions are not imposed (free).

Hybrid model has the same electron equations, while ions and neutrals are described via particle-in-cell method [22, 23, 38].

B. Role of boundary conditions and temperature evolution

Several characteristic features were observed with simulations in full fluid and hybrid models for $\nu_{\varepsilon,\mathrm{in}} = 0.4 \cdot 10^7$ s^{-1}. Generally, fluid and hybrid models show good agreement in the time averaged plasma parameters profiles, see Fig. 7. The agreement in the amplitude of the oscillating current and spectra are rather qualitatively similar but differ quantitatively, see Fig. 8.

The main cycle of low frequency (breathing mode) consists of several stages. The ions in the reverse electric field are moved relatively fast to the anode (~ 1 km/s). Then ions that reached the anode recombines and form peak in the neutral density near the anode, the enhanced density hump is advected into the ionization zone producing more ions. The ion density increases and fraction of ions is again moved to the anode, and the process repeats. Increasing v_a results in growth of oscillation frequency, approximately linearly. For $v_a = 150$ m/s the frequency is 10 kHz, which corresponds to neutral flyby time on the width of the ionization zone 1.5 cm observed in the simulations. Oscillations amplitude is also slightly increasing for larger neutral flow velocity.

The combination of the ion recycling on the anode side and temperature evolution are important for the low frequency oscillations. Ion recombination at the anode is included via the corresponding boundary condition for neutral atoms (26). When the ion recycling is turned the low-frequency oscillations disappear and the profiles are stationary. Low-frequency oscillations are sensitive to the ionization coefficient and they are not observed without the electron temperature evolution with fixed profile.

We have investigated how the magnitude of the anode boundary conditions affects the modes stability, Fig.10. The reduction of the absolute value of the velocity at the boundary reduces the amplitude of the oscillations, and below $0.6 \cdot c_s$ the oscillations disappear.

We also performed the simulations with higher energy losses $\nu_{\varepsilon,\mathrm{in}} = 10^7$ s^{-1} resulting in lower electron energy and oscillations of the lower amplitude, as shown in Fig.11. In it is interesting that for these parameters both methods show coexistence of low and high frequency modes, see Fig. 11.

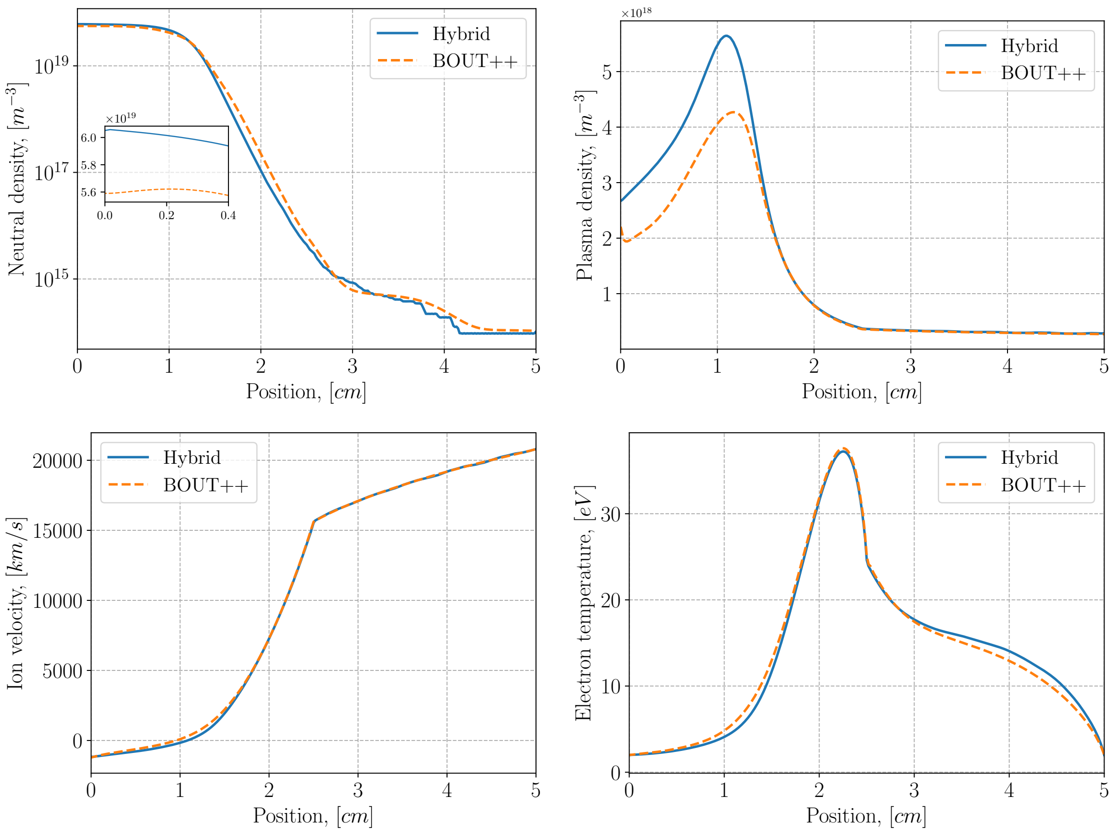

Fig. 7 Spatial distribution of time averaged macroscopic profiles from fluid and hybrid models for $\nu_\varepsilon = 0.4 \cdot 10^7$ s^{-1}.

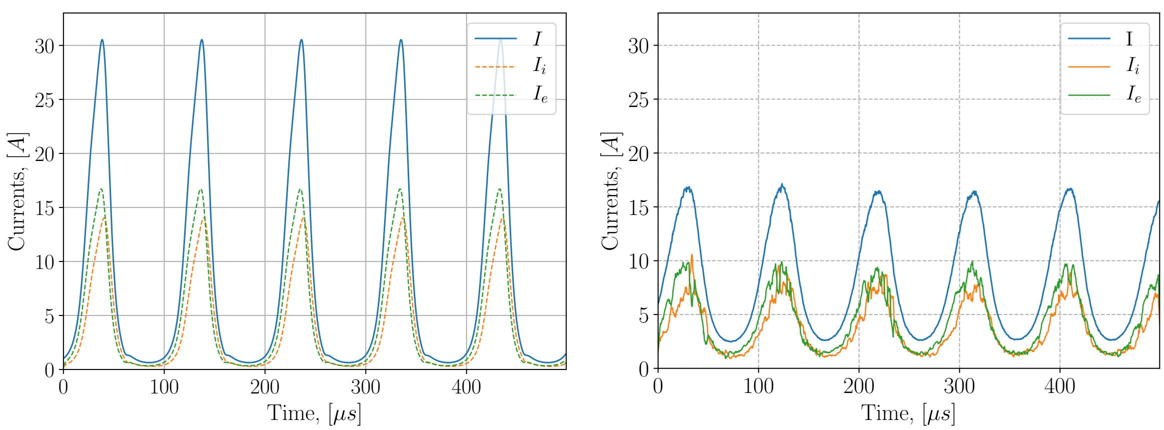

Fig. 8 Total, ion, and electron currents resulted from fluid model (left) and hybrid model (right) for $\nu_\varepsilon = 0.4 \cdot 10^7$ s^{-1}. Ion and electron currents are evaluated at $x = 5$ cm.

VI. Summary

Axial ionization modes involve the complex nonlinear dynamics of the ionization, ion acceleration, electron mobility, and diffusion. The interaction of these processes determines steady state profiles as well as spatial and temporal variations of the plasma density, ion velocity, neutral density, and total current.

Fluid models are based on the ion and electron density conservation (including ionization), ion momentum balance,

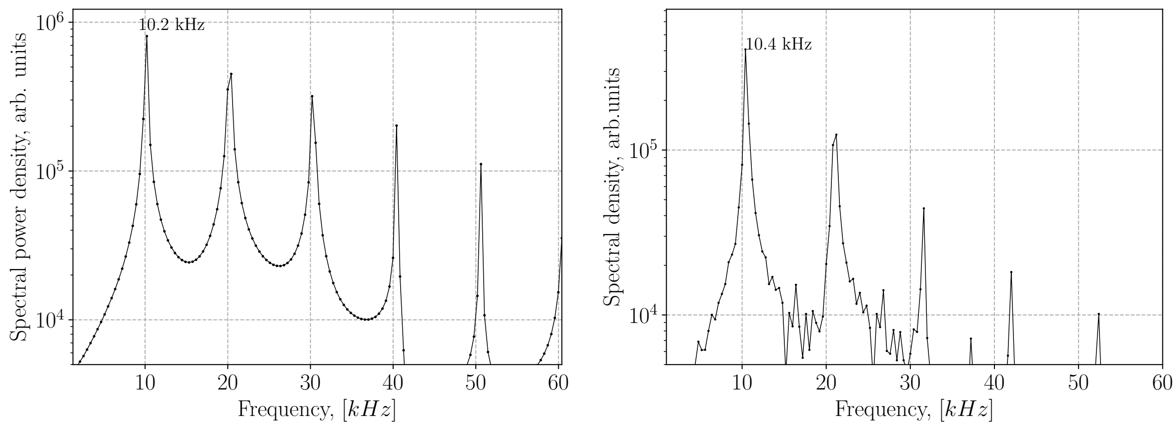

Fig. 9 Spectral density of the total current for fluid model (left) and hybrid model (right) for $\nu_\varepsilon = 0.4 \cdot 10^7$ s^{-1}.

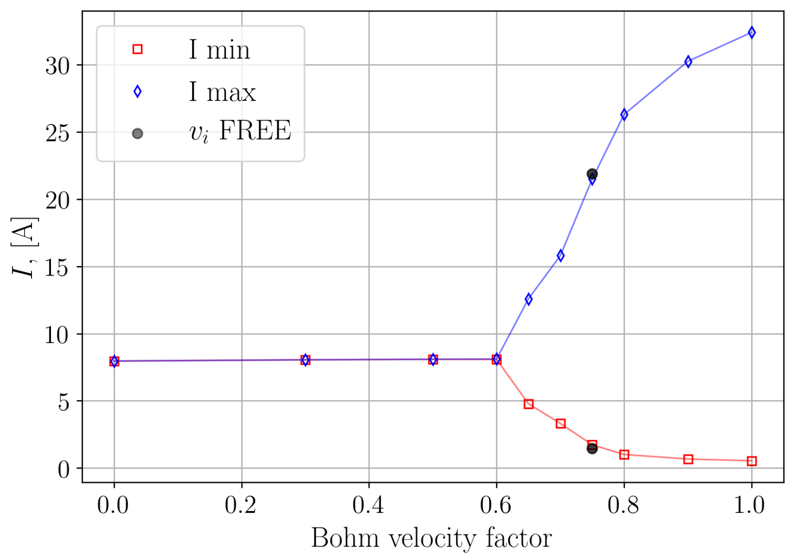

Fig. 10 Minimum and maximum values of the oscillating current for various ion velocities at the anode, expressed as fractions of the Bohm velocity. Note that oscillations are absent for $v_i < -0.6C_s$

and the electron flow in drift-diffusion approximation as well as the evolution of the electron energy. Fluid simulations of the quasi-neutral axial modes require boundary conditions imposed on the anode side as well as the condition for the electron temperature at the cathode. Different boundary conditions may exist at the anode sheath and quasineutral plasma interface.

In this paper, we study the nonlinear dynamics of the axial modes together with conditions for the existence of stationary solutions. The analysis of the stationary profiles show that there is a limited freedom in the choice of boundary condition due to global constraints imposed the regularization of the sonic point transition. For a simple case of uniform and constant temperature, fixed velocity of neutral injection, and without wall losses, we have semi-analytically determined the operational space diagram (in terms of the total current and mass injection rates).

The presence of the regularized sonic point makes steady-state plasma profiles rather stiff; therefore, the range of boundary conditions, where the solutions exist, may be limited. The operational space of the system parameters (total current, neutral flux, and plasma density) was investigated and was shown to have a complex structure. Analogous restrictions exist in more general case of the non-uniform temperature that will be reported elsewhere.

Our analysis shows that stability and characteristics of the axial modes are sensitive to the values of transport coefficients, boundary conditions, and the nature and parameters of the electron energy and its evolution. Stability

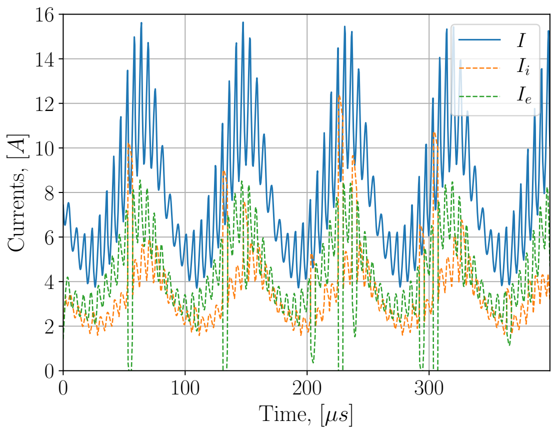

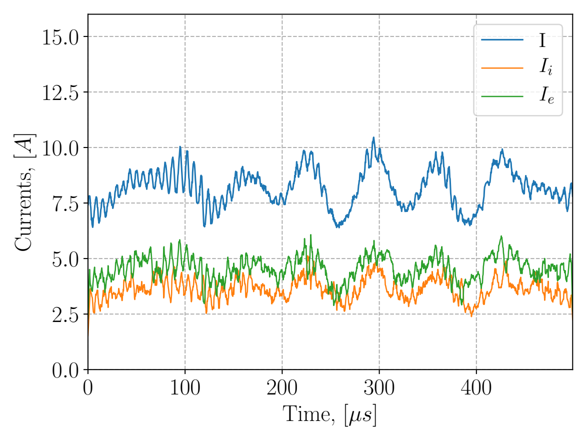

Fig. 11 Total, ion, and electron currents resulted from fluid model (left) and hybrid model (right) for $\nu_\varepsilon = 10^7\ s^{-1}$. Ion and electron currents are evaluated at $x = 5$ cm, $\nu_\varepsilon = 10^7\ s^{-1}$.

analysis of axial modes for a simplified case of uniform temperature and magnetic field with classical values of electron conductivity demonstrate the relatively high frequency (~100 kHz) oscillations (for magnetic field typical for CHT). The increase of the electron mobility and decreasing magnetic field in general result in reduction of frequency and even to disappearance of oscillations. Different oscillations patterns are identified (coherent, weakly coherent, and nonlinear) depending on the parameters of stationary solutions.

For the full model, when the electron energy equation is included, we have performed the comparison of the results from the fluid and hybrid modeling. The results from both methods are qualitatively similar but there are some quantitative differences in the oscillations amplitudes. Sensitivity to the boundary conditions, energy evolution and value of anomalous collisions and transport are identified in both approaches.

These results indicate importance of the self-consistent modeling of azimuthal and axial modes. Coupling between the two types of modes is expected because the azimuthal modes are driven by axial gradients in plasma parameters such as the density and electric field, which experience large spatial and temporal variations during breathing mode oscillations. In turn, axial modes are sensitive to the value of the anomalous transport produced by the azimuthal modes.

Acknowledgments

This work is supported in part by NSERC Canada, and US Air Force Office of Scientific Research FA9550-15-1-0226.

References

[1] J. M. Fife. *Hybrid-PIC Modeling and Electrostatic Probe Survey of Hall Thrusters*. Thesis, 1998.

[2] S. Barral and E. Ahedo. *On the origin of low frequency oscillations in Hall thrusters*, volume 993 of *Aip Conference Proceedings*, pages 439–442. 2008.

[3] K. Hara, M. J. Sekerak, I. D. Boyd, and A. D. Gallimore. Perturbation analysis of ionization oscillations in hall effect thrusters. *Physics of Plasmas*, 21(12), 2014.

[4] N. Yamamoto, T. Nakagawa, K. Komurasaki, and Y. Arakawa. Discharge plasma fluctuations in hall thrusters. *Vacuum*, 65(3-4):375–381, 2002.

[5] N. Yamamoto, K. Komurasaki, and Y. Arakawa. Discharge current oscillation in hall thrusters. *Journal of Propulsion and Power*, 21(5):870–876, 2005.

[6] N. Yamamoto, S. Yokota, K. Watanabe, A. Sasoh, K. Komurasaki, and Y. Arakawa. Suppression of discharge current oscillations in a hall thruster. *Transactions of the Japan Society for Aeronautical and Space Sciences*, 48(161):169–174, 2005.

[7] A. I. Morozov and V. V. Savel'ev. *International Electric Propulsion Conference, Moscow*, pages IEPC–95–161, 1995.

[8] A. I. Morozov and V. V. Savel'ev. One-dimensional hydrodynamic model of the atom and ion dynamics in a stationary plasma thruster. *Plasma Physics Reports*, 26(3):219–224, 2000.

[9] A. I. Morozov and V. V. Savel'ev. One-dimensional hybrid model of a stationary plasma thruster. *Plasma Physics Reports*, 26(10):875–880, 2000.

[10] J. P. Boeuf and L. Garrigues. Low frequency oscillations in a stationary plasma thruster. *Journal of Applied Physics*, 84(7):3541–3554, 1998.

[11] S. Chable and F. Rogier. Numerical investigation and modeling of stationary plasma thruster low frequency oscillations. *Physics of Plasmas*, 12(3):033504, 2005.

[12] E. Fernandez, M. K. Scharfe, C. A. Thomas, N. Gascon, and M. A. Cappelli. Growth of resistive instabilities in exb plasma discharge simulations. *Physics of Plasmas*, 15(1):012102, 2008.

[13] O. Koshkarov, A. I. Smolyakov, I. V. Romadanov, O. Chapurin, M. V. Umansky, Y. Raitses, and I. D. Kaganovich. Current flow instability and nonlinear structures in dissipative two-fluid plasmas. *Physics of Plasmas*, 25(1):011604, 2018.

[14] S. Barral, K. Makowski, Z. Peradzynski, and M. Dudeck. Transit-time instability in hall thrusters. *Physics of Plasmas*, 12(7), 2005.

[15] Z. Peradzynski, K. Makowski, S. Barral, J. Kurzyna, and M. Dudeck. *The role of the electron energy balance in plasma thruster instabilities*, volume 993 of *Aip Conference Proceedings*, pages 435–438. 2008.

[16] S. Barral and E. Ahedo. Low-frequency model of breathing oscillations in Hall discharges. *Physical Review E*, 79(4), 2009.

[17] S. Barral and Z. Peradzynski. Ionization oscillations in Hall accelerators. *Physics of Plasmas*, 17(1), 2010.

[18] L. Q. Wei, L. Han, D. R. Yu, and N. Guo. Low-frequency oscillations in hall thrusters. *Chinese Physics B*, 24(5):055201, 2015.

[19] C. Wang, L. Wei, and D. Yu. A basic predator-prey type model for low frequency discharge oscillations in hall thrusters. *Contributions to Plasma Physics*, 51(10):981–988, 2011.

[20] E. T. Dale, B. A. Jorns, and K. Hara. Numerical investigation of the stability criteria for the breathing mode in hall effect thrusters. *35th International Electric Propulsion Conference*, pages IEPC–2017–2265, October 8–12 2017.

[21] D. Eckhardt, J.W. Koo, and D.B. Scharfe. *35th International Electric Propulsion Conference*, pages IEPC–2017–2540, 2017.

[22] G. J. M. Hagelaar, J. Bareilles, L. Garrigues, and J. P. Boeuf. Modelling of stationary plasma thrusters. *Contributions to Plasma Physics*, 44(5-6):529–535, 2004.

[23] G. J. M. Hagelaar, J. Bareilles, L. Garrigues, and J. P. Boeuf. Two-dimensional model of a stationary plasma thruster. *Journal of Applied Physics*, 91(9):5592–5598, 2002.

[24] K. Hara and I. G. Mikellides. *Characterization of low frequency ionization oscillations in Hall thrusters using a one-dimensional fluid model*. 2018.

[25] A. Shashkov, A. Lovtsov, and D. Tomilin. A one-dimensional with three-dimensional velocity space hybrid-pic model of the discharge plasma in a hall thruster. *Physics of Plasmas*, 24(4):043501, 2017.

[26] S. Barral, Z. Peradzyski, K. Makowski, and M. Dudeck. Fluid model of hall thruster - comparison with hybrid model. *High Temperature Material Processes*, 5(2):253–263, 2001.

[27] E. Ahedo, P. Martinez-Cerezo, and M. Martinez-Sanchez. One-dimensional model of the plasma flow in a hall thruster. *Physics of Plasmas*, 8(6):3058–3068, 2001.

[28] A. Cohen-Zur, A. Fruchtman, J. Ashkenazy, and A. Gany. Analysis of the steady-state axial flow in the hall thruster. *Physics of Plasmas*, 9(10):4363–4374, 2002.

[29] E. Ahedo, J. M. Gallardo, and M. Martinez-Sanchez. Model of the plasma discharge in a hall thruster with heat conduction. *Physics of Plasmas*, 9(9):4061–4070, 2002.

[30] L. Dorf, V. Semenov, and Y. Raitses. Anode sheath in hall thrusters. *Applied Physics Letters*, 83(13):2551–2553, 2003.

[31] A. Bers. Space-time evolution of plasma instabilities - absolute and convective. In *Handbook of Plasma Physics, Basic Plasma Physics*. North-Holland, Amsterdam, 1984.

[32] A. Fruchtman, N. J. Fisch, and Y. Raitses. Control of the electric-field profile in the Hall thruster. *Physics of Plasmas*, 8(3):1048–1056, 2001.

[33] Ivan Romadanov et al. *Theoretical and experimental studies of large scale modes in Hall thrusters and methods of their control*. PhD thesis, University of Saskatchewan, 2019.

[34] E. Ahedo and J. Rus. Vanishing of the negative anode sheath in a hall thruster. *Journal of Applied Physics*, 98(4):043306, 2005.

[35] E. Ahedo, R. Santos, and F. I. Parra. Fulfillment of the kinetic bohm criterion in a quasineutral particle-in-cell model. *Physics of Plasmas*, 17(7), 2010.

[36] L. Dorf, Y. Raitses, and N. J. Fisch. Experimental studies of anode sheath phenomena in a hall thruster discharge. *Journal of Applied Physics*, 97(10):–, 2005.

[37] B.D. Dudson, M.V. Umansky, X.Q. Xu, P.B. Snyder, and H.R. Wilson. BOUT++: A framework for parallel plasma fluid simulations. *Computer Physics Communications*, 180(9):1467 – 1480, 2009.

[38] G. J. M. Hagelaar, J. Bareilles, L. Garrigues, and J. P. Boeuf. Role of anomalous electron transport in a stationary plasma thruster simulation. *Journal of Applied Physics*, 93(1):67–75, 2003.

[39] Low temperAture magNetizeD plasMA benchmaRKs. `https://www.landmark-plasma.com/`.